Small eukaryotic phytoplankton can play an outsized role in carbon export in iron-limited regions

Meredith G. Meyer[1], Vincent J. White[1], Olivia Torano[1], Heidi Hannoush[1], and Adrian Marchetti[1]

[1]Department of Earth, Marine, and Environmental Sciences, University of North Carolina at Chapel Hill, Chapel Hill, NC, USA

To be submitted to: ISME Journal
July 1, 2024

Corresponding Author: A. Marchetti (amarchetti@unc.edu)

The authors declare no competing interests.

Abstract

Small eukaryotic phytoplankton can account for considerable amounts of biomass and primary production in high nutrient, low chlorophyll (HNLC) regions of the ocean where iron-limitation is pronounced. However, the strategies these cells invoke to cope under low iron conditions and the extent to which they are responsible for new production (i.e., the fraction of primary production supported by nutrients from outside of the euphotic zone) is unclear. Here, we examine how a representative picoeukaryote, the chlorophyte *Bathycoccus sp*., recently isolated from the iron-limited subarctic North Pacific Ocean, responds to iron-limitation and quantify its potential contribution to carbon export. Iron-limited *Bathycoccus* exhibits reductions in cellular growth rate, volume, and carbon and nitrogen quotas along with a restructuring of cellular metabolism. Gene expression and pathway analyses show evidence of cellular strategies to mitigate iron limitation but constitutive expression of genes related to nitrogen uptake and utilization. Additionally, when grown on nitrate, cellular carbon and nitrogen quotas ranged from 0.02 – 0.17 pmol C $cell^{-1}$ and 3.3×10^{-3} – 2.2×10^{-2} pmol N $cell^{-1}$, respectively, as a function of iron status. Based on the measured cellular quotas, we estimate that representative picoeukaryotes, such as *Bathycoccus*, in HNLC North Pacific waters can account for a majority of new production under ambient iron-limited conditions, supporting the need for a paradigm shift in our thinking of the role small eukaryotic phytoplankton play in the global carbon cycle.

1. Introduction

In open-ocean systems, high surface area-to-volume ratios and generally lower nutrient quotas make eukaryotic picophytoplankton strong competitors for nutrients, thus enabling them to routinely dominate these oligotrophic environments (Worden and Not, 2008). While much research has focused on cyanobacteria, specifically *Prochlorococcus* (Chisholm et al., 1991) and *Synechococcus* (Moore et al., 2002), fewer studies have investigated the growth strategies of picoeukaryotes which have been shown to potentially play key ecological roles as well (Fowler et al., 2020). Previous studies have suggested chlorophytes and other small eukaryotic groups primarily rely on ammonium and other forms of recycled nitrogen to support their growth (Greene et al., 1992; Marchetti et al, 2006; Meyer et al., 2022). Compared to cyanobacteria, diatoms, and dinoflagellates, these picoeukaryotes are poorly characterized and are less likely to be available in culture. Thus, there are fewer monocultured representatives sequenced for genomic and/or transcriptomic analyses compared to other phytoplankton groups (Le Gall et al., 2008). This overall lack of knowledge has led to these organisms commonly being overlooked in whole community analyses despite their high abundances.

Given the potentially outsized role these eukaryotic picophytoplankton could play in oligotrophic and nutrient-limited regions, understanding the nutrient acquisition strategies and metabolisms employed by these phytoplankton and the resultant effect for general ecosystem productivity and carbon export potential is of substantial importance. Here we present measurements obtained from the chlorophyte, *Bathycoccus sp.*, that was recently isolated from Ocean Station Papa (Station P) in the subarctic North Pacific during the NASA EXport Processes in the Ocean from RemoTe Sensing (EXPORTS) program in 2018. *Bathycoccus sp.* is an abundant member of the *Mamiellales* order and is closely related to *Micromonas* and *Ostreococcus* (Monier et al., 2016; Vannier et al., 2016), two other

ecologically important picoeukaryotes. While studies have shown that *Bathycoccus* can occupy a wide range of habitats and exhibits an “occupy-abundance pattern” (i.e., *Bathycoccus* frequently becomes one of the most abundant genera in regions where they are present; Monier et al., 2016), metabolic capabilities and the ecological role of *Bathycoccus* is still poorly understood.

Station P is the site of a long-term monitoring program which resides within a High Nutrient (predominantly nitrate (NO_3^-)), Low Chlorophyll, or HNLC, region. This region experiences chronic limitation of iron bioavailability which, despite replete macronutrient concentrations, inhibits substantial phytoplankton biomass standing stock and higher rates of primary production (Martin et al., 1988; Marchetti et al., 2006). Iron is used as a crucial co-factor in photosynthesis and nitrogen assimilation (LaRoche et al.,1993; Peers and Price, 2006). Many groups of phytoplankton that experience iron limitation have been shown to utilize regenerated nitrogen sources (e.g., ammonium (NH_4^+) or urea) which theoretically have a lower iron requirement relative to oxidized forms of nitrogen or nitrogen gas (Price et al., 1994; Varela and Harrison, 1999). In addition, recent findings suggest that the dominant cyanobacteria in the North Pacific, *Synechococcus*, lacks the necessary pathways for NO_3^- acquisition and assimilation, thus being restricted to regenerated production (Sharpe et al., 2023). This finding presents a knowledge gap in our understanding of which organisms are responsible for the vast majority of new production in the region, which has routinely been measured to be driven predominantly by small phytoplankton less than 5 µm in cell diameter (Meyer et al. 2022).

Here, we contribute to the understanding of picoeukaryotes such as *Bathycoccus* through determining rates of cellular growth, photophysiology, carbon and nitrogen content, and trends in gene expression of cells as a function of iron status. Quantifying elemental requirements and the response to iron limitation of key phytoplankton groups in the ocean is

critical for elucidating the ecology and biogeochemistry of vast regions of the global ocean under current and future climate scenarios.

2. Methods

2.1 Sampling and Cell Isolation

Whole seawater was collected via a trace metal clean rosette during the NASA EXport Processes in the Ocean from RemoTe Sensing (EXPORTS) field campaign to Ocean Station Papa (Station P) in the subarctic North Pacific. This campaign occurred from August 16th, 2018 to September 7th, 2018. Sampled seawater was stored in culture flasks and incubated in on-deck incubators before being transported back to the University of North Carolina for cell isolation. An abundant, small (< 5 µm) chlorophyte was isolated using a 10 µL pipette. DNA was extracted using standard protocols with a DNEasy Plant Mini Kit (Qiagen). The 18S rRNA gene was sequenced, and forward and reverse reads searched against the National Center for Biotechnology Information (NCBI) repository using BLAST, revealing the highest sequence similarity to *Bathycoccus sp*. (accession number XR_002608757) with a 97.7% percent ID and 88% query cover.

2.2 Culture conditions

Bathycoccus sp. cells were maintained in Aquil media in an incubator under constant 120-150 µmol photons m^{-2} s^{-1} light at 12ºC. To examine the effects of differing nitrogen forms and iron states on *Bathycoccus* growth and physiology, four trace metal clean culture treatments were initiated. Aquil medium was sterilized in a microwave, cooled, and supplemented with filter-sterilized (0.2-µm Acrodisc) ethylenediamene tetraacetic acid (EDTA) trace metals (minus iron), vitamins (B_{12}, thiamine, and biotin), and chelexed macronutrients (NO_3^-, PO_4^{3-}) in accordance with Aquil medium concentrations (Price et al.

1989). Trace-metal concentrations were buffered using 100 mmol L^{-1} of EDTA. Two treatments contained NO_3^- (300 µM) and two treatments contained NH_4^+ (30 µM) as their nitrogen source. Within each nitrogen treatment, there was an iron replete (1370 nM total Fe) and an iron deplete (3.1 nM total Fe) treatment. Thus, the four treatments can be described as NO_3^- Fe+, NO_3^- Fe-, NH_4^+ Fe+, and NH_4^+ Fe-. Each treatment was first cultured in triplicate acid-washed 28 mL clear, polycarbonate centrifuge tubes (Nalgene, Rochester, NY) for acclimation to their respective treatments. Cells were acclimated to their treatment for a minimum of three transfers before experiments began. During acclimation, 200 µL of dense late exponential-phase culture was transferred to new tubes with fresh media to maintain growth. Following acclimation, cultures were transferred to a trace metal clean, 1 L polycarbonate bottle that was approximately 700 mL full. NH_4^+ Fe+ and NH_4^+ Fe- cultures were not able to maintain stable growth, thus confining our experiment to the NO_3^- Fe+ and NO_3^- Fe-, referred to as Fe+ and Fe- treatments herein. All culture preparation, maintenance, and cell transfers were conducted under a positive-pressure, trace metal clean laminar flow hood.

During the experiments, approximate cell growth and concentrations were monitored via relative fluorescence units (RFUs) on a Turner 10AU fluorometer from lag phase through stationary phase (Brand et al. 1981). Once samples were determined to be in mid-exponential phase, cultures were measured for RFUs and the Fv/Fm using a Satlantic FIRe fluorometer (see below) and harvested for cell counts, chlorophyll *a* (Chl *a*) concentration, particulate carbon (C) and nitrogen (N) concentration, and RNA. Harvest volumes were approximately 1.8 mL, 50 mL, 100 mL, 15 mL, and 200-300 mL for cell counts, Chl *a* concentration, particulate carbon (PC) and particulate nitrogen (PN) concentration, culture media nutrients, and RNA, respectively.

Growth rates (μ) were calculated according to the method of Brand et al. (1981). Assuming Fe+ represents a maximum growth rate (μ_{max}), the ratio of average μ/μ_{max} (i.e., Fe-/Fe+) can be calculated. The maximum quantum yield of photochemistry in photosystem II (PSII; Fv/Fm) and the functional absorption cross section of PSII (σ_{PSII}) were measured as metrics to evaluate photosynthetic efficiency (Gorbunov and Falkowski; 2004).

Chl *a* was analyzed following Graff and Rynearson (2011). Particulate carbon (PC) and nitrogen (PN) were analyzed on a Carlo Erba NC 2500 elemental analyzer at University of Maryland Center for Environmental Science Appalachian Laboratory in Frostburg, Maryland. Cultures for RNA were filtered onto an Isopore 0.4 µm pore size, 47 mm polycarbonate filter under gentle vacuum pressure and stored at -80 ºC before extraction. RNA was extracted using standard protocols with a RNAqueous-4PCR kit at the University of North Carolina. Filters were treated with a lysis buffer/ethanol solution, wash solution, secondary (2/3rd) wash solution, and elution (lysis) solution. After each addition, the resulting solution was added to the filter column and centrifuged at 16,000 x g for 1 minute (at one step 5 minutes). Extracted RNA was checked for quality (A280/260, A260/230, and nucleic acid concentration) on a Nanodrop spectrophotometer and cleaned up via a RNeasy MinElute Clean-up kit. RNA was sent to the Azenta Genewiz Sequencing Facility in South Plainfield, New Jersey for Illumina high throughput analysis with ~350M raw paired-end reads per lane and single index, 2 x 150 bp per lane, resulting in a read depth of 148.85 million reads per sample, on average.

2.3 Cell counts and size estimates

A small aliquot (1.8 mL) of each culture (both treatments and all replicates) were preserved in 200 µL of paraformaldehyde (pFa) in 2 mL cryovials at the time of cell harvest, the day following the harvest and several (2-3) days preceding the harvest. Cryovials were immediately flash frozen in liquid nitrogen and stored at -80ºC until they were analyzed on a

Guava easyCyte flow cytometer equipped with a red laser in the Paerl Lab at North Carolina State University. Data was processed by InCyte software to provide cell counts based on red fluorescence. Estimates of cell size were also calculated using calibration beads of known size based on the relationship of Paerl et al. (2020). Chl *a* concentrations and PC and PN quotas per cell were calculated by normalizing concentrations to cell counts per culture.

2.4 North Pacific new production calculations

If we assume *Bathycoccus* is a representative proportion of the picoeukaryote population at Station P, upper bound estimates of the contribution of picoeukaryotes to total new production under Fe-replete and Fe-limiting conditions can be calculated according to Equation 2:

$$New\ production = cell\ concentration * \mu * N\ quota \qquad \text{(Eq. 2)}$$

Where the nitrogen quota is in units of pmol N $cell^{-1}$. Here, the N quota and μ come from our experimental results with the *Bathycoccus* culture whereas the cell count is the sampling day average picoeukaryote cell count (3.3×10^6 cells L^{-1}) in the surface waters at Station P from flow cytometry measurements collected aboard the EXPORTS cruise (see McNair et al. (2023) for further details).

2.5 Gene expression analysis

Transcripts were trimmed of sequence adapters and poly-A tails via Trim_galore (v.0.6.2; Altos Labs) and underwent quality control analysis via FastQC (v.0.11.9) where sequences with a quality score below 20 and/or length less than 50 base pairs were removed. Merged sequence files were assembled de novo via Trinity (v.2.8.6) before being combined into grand assemblies based on iron treatment via cdhit (v.4.8.1; Fu et al., 2012). Sequences underwent functional annotation via the Kyoto Encyclopedia of Genes and Genomes (KEGG;

Release 88.2). Additional manual annotation of genes associated with Fe metabolism but are not included in KEGG (e.g., rhodopsins, iron starvation induced proteins (ISIPs), and phytotransferrins) was conducted (see Moreno et al., 2017 for more information on manual annotation and sequence acquisition). Independent end-to-end read alignment occurred via Salmon (v.10.9.1; Patro et al., 2017) and annotation and count files were combined via tximport, providing counts per million (CPM) values per gene per sample (Soneson et al., 2015). Differential expression of genes was analyzed at the KEGG Ortholog (KO) level, averaging values for multiple contigs with the same KO, according to the DESeq2 package in RStudio (v.4.2.2). The Log2Fold change (adjusted p-value <0.05) of specific genes of interest, particularly those associated with photosynthesis, N metabolism, and Fe metabolism, were investigated. Additionally, trends in KEGG metabolic pathways were analyzed among samples. Figures were generated in Matlab R2022b. Sequences from this analysis are available at the National Center for Biotechnology Information (Ascension numbers: SAMN39858273 - 284).

3. Results

3.1 Growth rates and photosynthetic efficiency

The Fe+ cultures had an average growth rate of 0.96 ± 0.01 d^{-1}. The average growth rate of Fe- cultures was substantially lower at 0.48 ± 0.07 d^{-1} resulting in a μ/μ_{max} (Fe-/Fe+) of 0.50, suggesting substantial limitation of iron in the Fe- treatment relative to the Fe+ treatment. Estimates of maximum photochemical yield of PSII (Fv/Fm) confirm that the Fe+ cultures were healthy whereas Fe- was experiencing iron-limited conditions. The mean Fv/Fm for the Fe+ treatment was 0.73 ± 0.02, whereas values for the Fe- cultures were 0.37 ± 0.03, consistent with a decline in photosynthetic efficiency of PSII due to iron limitation (Fig. 1B). Multiple analyses (Fv/Fm, growth rates, etc.) produced substantially different results for

the Fe+ Triplicate A sample, suggesting this replicate was physiologically distinct from Fe+ triplicates B and C. Specifically, Fe+ A had a low Fv/Fm value of 0.27, suggesting that this culture was already in stationary phase and experiencing nutrient depletion at the time of sampling. This triplicate was therefore removed from the averages of Fe+ sample data.

The cross-sectional absorption area of photosystem II (σ) was also consistent with other iron-limited phytoplankton cultures with an increase in σ under iron-limited conditions (Ellis, 2015; Moreno et al., 2020). For Fe- cultures, σ averaged 1036 ± 264, and for Fe+, σ averaged 372 ± 12 (Fig. 1C), resulting in a 2.8-fold increase under iron-limited conditions.

3.2 Cell Size

The Fe+ cultures had an average cell diameter of 1.85 ± 0.02 µm and corresponding cell volume of 3.35 ± 0.10 μm^3 (Fig. 1). The Fe- cultures had an average cell diameter of 1.58 ± 0.00 µm and cell volume of 2.07 ± 0.00 μm^3 (Fig. 1). However, Fe- cultures had a higher cell density of $1.24 \times 10^{10} \pm 7.08 \times 10^{8}$ cells L^{-1} whereas Fe+ cultures had a density of $1.96 \times 10^{9} \pm 5.84 \times 10^{7}$ cells L^{-1}.

3.3 Chlorophyll a content

Cellular Chl *a* contents exhibited an order of magnitude difference between the Fe+ and Fe- samples, with the Fe+ cultures having an average of $6.42 \times 10^{-6} \pm 5.01 \times 10^{-7}$ ng $cell^{-1}$ and the Fe- cultures averaging only $5.27 \times 10^{-7} \pm 8.68 \times 10^{-8}$ ng $cell^{-1}$. Chl *a* concentration, when normalized to cell biovolume as described above, exhibited a similar trend to cellular content, but the difference in the magnitude between the Fe+ and Fe- cultures was substantially lower. The average Fe+ was $1.92 \times 10^{-6} \pm 9.12 \times 10^{-8}$ ng μm^{-3} whereas the average Fe- biovolume-normalized cellular content was 7.5-fold lower at $2.54 \times 10^{-7} \pm 4.18 \times 10^{-8}$ ng μm^{-3}.

3.4 Cellular carbon and nitrogen quotas

Like Chl *a*, the cellular C content exhibited an order of magnitude difference between the Fe+ and Fe- treatments. The Fe+ cultures had a high cellular C quota of 0.16 ± 0.02 pmol C $cell^{-1}$ whereas the Fe- cultures had an 8-fold lower C quota of 0.02 ± 0.00 pmol C $cell^{-1}$ (Fig. 2A). As is seen throughout the parameters measured, the Fe- sample quotas were consistent, only ranging from 0.022 – 0.024 pmol C $cell^{-1}$ among triplicates. When normalized to cell volume, the biovolume-normalized C quotas were more similar between treatments due to the cells in the Fe+ culture being ~1.5-fold larger than the cells in the Fe- culture. The Fe+ treatment had a C quota of $4.73 \times 10^{-2} \pm 3.80 \times 10^{-3}$ pmol C μm^{-3} whereas the quota for the Fe- treatment was $1.11 \times 10^{-2} \pm 3.82 \times 10^{-4}$ pmol C μm^{-3} (Fig. 2B). Thus, when considering the difference in cell volumes (i.e., calculated per μm^{-3} rather than per cell), the difference in C quota decreases from 8.0- to 4.3-fold higher in the Fe+ treatment relative to the Fe- treatment.

The cellular N contents likewise exhibited orders of magnitude differences between iron treatments when normalized per cell and per unit volume. The average N quota for the Fe+ cultures was $2.11 \times 10^{-2} \pm 1.51 \times 10^{-3}$ pmol N $cell^{-1}$ whereas the average for the Fe- cultures was $3.37 \times 10^{-3} \pm 1.33 \times 10^{-4}$ pmol N $cell^{-1}$ (Fig. 2C). The per unit volume average for Fe+ samples was $6.30 \times 10^{-3} \pm 2.58 \times 10^{-4}$ pmol N μm^{-3}, and for the Fe- samples was $1.62 \times 10^{-3} \pm 6.44 \times 10^{-5}$ pmol N μm^{-3} (Fig. 2D). The change in cellular N contents as a function of iron status was similar to that of C at approximately 6- and 4-fold larger for the Fe+ treatment when normalized per cell and per unit volume, respectively. Both treatments exhibited slightly higher particulate carbon : nitrogen (C:N) ratios than the Redfield ratio of 6.6 with averages of 7.49 ± 0.30 and 6.84 ± 0.05 for Fe+ and Fe-, respectively (Fig. 2E). C:Chl *a*

ratios exhibited the opposite pattern with a higher average ratio (537 ± 111 µg : µg) in the Fe- treatment than in the Fe+ treatment (296 ± 9.74 µg : µg; Fig. 2F).

3.5 Potential contributions to new production in the NE Pacific

Rates of potential contributions to new production varied by an order of magnitude between iron treatments, averaging 5.4 ± 1.0 nmol N L^{-1} d^{-1} for Fe- cultures and 67.5 ± 4.3 nmol N L^{-1} d^{-1} for Fe+ cultures (Fig. 3). Rates were highly variable, with Fe- values ranging from 3.7 to 8.4 nmol N L^{-1} d^{-1} and Fe+ values ranging from 45.9 to 105.1 nmol N L^{-1} d^{-1}. Rates of small-celled new production at Station P were always between the Fe- and Fe+ rates, except for on YD 240 when the EXPORTS rate was higher than Fe+ (55.4 nmol N L^{-1} d^{-1}) at 58.5 nmol N L^{-1} d^{-1}. The average picoeukaryote cell concentration during the EXPORTS observation period used in these calculations was 3.34 x 10^6 cells L^{-1} (see https://seabass.gsfc.nasa.gov/cruise/EXPORTSNP/ for data).

3.6 Gene expression

Molecular sequencing of the *Bathycoccus sp.* transcriptome indicated a higher GC content for the Fe+ (61%) vs. Fe- (49%) cultures. Total sequences and sequence length were comparable between treatments at 6.51 x 10^7 vs. 6.19 x 10^7 sequences and 148.90 vs. 148.81 mbp per Fe+ and Fe-, respectively.

The impact of Fe availability was analyzed broadly on the metabolic pathway level (Fig. 4A) and specifically on a targeted gene level (Fig. 4B). Of the 17 metabolic pathways of interest analyzed, on average, 10 displayed enhanced expression under Fe- conditions (i.e., negative Log2Fold change). Key pathways exhibiting this trend include those related to iron limitation mitigation strategies or general physiological stress response, including iron starvation induced protein expression, ferredoxin expression, higher expression of

photosystem I relative to photosystem II, and zeaxanthin epoxidase (Fig. 4A). Unsurprisingly, many gene transcripts involved in pathways related to general cell maintenance, including nitrogen metabolism, arginase, flavin adenine dinucleotide synthesis, etc., were overrepresented under Fe+ conditions.

Evaluating these physiological trends further, our findings appear consistent with those previously reported for the closely-related chlorophyte, *Ostreococcus* (Lelandis et al., 2016), with *Bathycoccus* appearing to contain far fewer transcribed genes involved in nitrogen and iron metabolism than are commonly reported in diatoms and other phytoplankton taxa. Transcripts for the nitrogen assimilation genes nitrate/nitrite transporters (*NRT*), nitrate reductase (*NR*), nitrite reductase (*NiR*), ammonium transporters (*AMT*), and urea transporters (*Urt*) were identified in *Bathycoccus* (Fig. 4B, 4C). Most genes associated with NO_3^- uptake (*NRT*, *NiR*) increased expression (Log2Fold changes > 0) in the Fe+ treatment relative to Fe- treatment (Fig. 4B). Urea transporters were also overrepresented (Log2Fold change = 4.21; adjusted p-value < 0.01) under Fe+ conditions. Conversely, ammonium transporters showed a slight negative Log2Fold change (-0.47), suggesting increased expression in the Fe- treatment (Fig. 4B, 4C). Overall, genes associated with the expression of photosystems I and II (*Psa*, *Psb*) exhibited a stronger Log2Fold change (-2.93) in Fe- conditions, in contrast to the common assumption that these photosynthetic genes should be more highly expressed under iron-replete conditions (Fig. 4B).

Our data suggests that *Bathycoccus* may lack genes commonly involved in iron regulation and homeostasis in HNLC regions, including proton-pumping rhodopsins and ferritin. It did, however, show the presence of one iron starvation induced protein (*ISIP3*) which was strongly expressed (Log2Fold change = -4.62; adjusted p-value <0.01) under Fe- conditions (Fig. 4B). The percent of overall contigs without a functional annotation was high

(87.9%), suggesting additional genes involved in both nitrogen and iron metabolism may be present but are not identified in the KEGG database.

4. Discussion

4.1 Cellular and metabolic characterization

While less is known about the ecology and physiology of *Bathycoccus sp.* relative to other picoeukaryotic chlorophytes such as *Micromonas* and *Ostreoccocus*, our findings reported here are consistent with and build upon what has generally been reported on *Bathycoccus sp*. Our estimates of cell size fall within the reported range from 1.5 – 2.5 µm (Vannier et al., 2016). Additionally, *Ostreoccocus* has been reported to exhibit fast growth rates (0.62 – 1.14 d^{-1}; Worden et al., 2004), consistent with our measured growth rates for *Bathycoccus* in iron-replete conditions. However, a substantial lag phase has not been previously reported. Additionally, our inability to grow *Bathycoccus* in a consistent manner to higher biomass using NH_4^+ media is noteworthy. While we were unable to identify what was inhibiting growth, it is likely that *Bathycoccus* requires specific conditions for NH_4^+ utilization that were not present within our culture conditions. Our findings suggest that *Bathycoccus* may exhibit a similar preference for NO_3^- over other forms of nitrogen (such as NH_4^+), but further research into this topic is warranted.

Our study is the first we are aware of that quantified changes in cellular Chl *a* concentration and C and N quotas in iron-replete and deplete *Bathycoccus sp.* cells. Understanding these iron limitation-driven differences is critical as changes in growth rates and elemental quotas of *Bathycoccus* may have ecosystem and biogeochemical implications in HNLC regions. Consistent with current paradigms from diatoms, iron-replete *Bathycoccus* were larger, had higher growth rates, higher cellular Chl *a* content, and appreciably higher C

and N quotas relative to their iron-limited counterparts. Although the Fe-limited cells were smaller with lower growth rates and cellular quotas, they were able to reach higher cell densities. Under both iron conditions, *Bathycoccus* experienced a substantial lag growth period suggesting that *Bathycoccus sp*. are not quick to respond to pulses of iron availability like some larger phytoplankton, specifically diatoms (Marchetti et al., 2006). This is consistent with our observation of how abundant these cells were in the Northeast Pacific, suggesting *Bathycoccus* is a genera more likely to be found under the chronic, iron-limited HNLC environment rather than during periods of pulsed iron bioavailability.

4.2 Iron limitation strategies

Our findings are in line with previous work (Martin and Fitzwater, 1988; Boyd et al., 1998; Marchetti et al., 2006) suggesting low Fe concentrations limit nitrate uptake as is supported by a low relative growth rate (μ/μ_{max}). This leads to substantially curtailed growth rates, and trends in gene expression where genes involved in nitrate metabolism (e.g., *NRT*, *NiR*) are more highly expressed under iron-replete conditions. Our gene expression data supports the hypothesis that *Bathycoccus* is an important contributor to new production, showing clear expression patterns in genes involved in NO_3^- metabolism coinciding with their ability to grow effectively on NO_3^-. *Bathycoccus* also appears capable of urea metabolism by expressing urea transporters in addition to *NiR* and *NRT*. A similar finding was reported by Piganeau et al. (2011) where the closely related *Micromonas* exhibited selective pressure for nitrate and urea uptake, but not ammonium uptake. This finding is consistent with our inability to establish steady-state growth when cells were grown in NH_4^+ based media. However, this is paradoxical given the need to reduce NO_3^- to NH_4^+ for utilization in photosynthesis and the lower energetic cost of NH_4^+ utilization relative to NO_3^- utilization (Raven, 1988). Cultures were able to grow sporadically on NH_4^+, but stable

growth was not achieved. This, combined with the presence of *AMT* in the transcriptome, suggests *Bathycoccus* have the physiological capabilities for NH_4^+ utilization but were perhaps inhibited by some external factor, such as a vitamin or a micronutrient.

The lack of information on iron regulation is consistent with findings from previous studies of *Ostreococcus* (Lelandais et al., 2016). The majority of what is known about phytoplankton iron metabolism comes from studies of diatoms (Peers and Price, 2006; Marchetti et al., 2012), and thus, most of the genes annotated for iron metabolism present in KEGG are from diatoms. It is not surprising that many of the iron transport and homeostasis genes identified in diatoms were not readily identified in *Bathycoccus* given the substantial physiological differences between the two phytoplankton groups. The only iron-related gene identified and present in our iron transport model is ISIP3. However, as is noted by Lelandais et al. (2016) for *Ostreococcus*, the high percentage of unannotated genes in our strain suggests that chlorophytes likely have novel methods for dealing with iron limitation which have not yet been well characterized. Currently, a Ton-B receptor gene has been sequenced from a *Bathycoccus sp.* and is available on NCBI (Ascension number: XP_007508231.1). While this gene is not present in our cultures, it is a target gene that should be investigated in future studies. Our study represents the first analysis of this species from an HNLC region. Previous studies have shown *Bathycoccus* can adapt quickly to variable environmental conditions, gaining or losing genes based on physical changes, which may suggest the species studied here exhibits physiological characteristics and adaptations that are very different from what is currently characterized in the scientific literature (Vannier et al., 2016).

An additional, noteworthy finding is that our data appears to suggest that *Bathycoccus* exhibit a form of nitrogen metabolism conservation even under Fe replete conditions. The gene expression analysis demonstrates most genes related to nitrogen metabolism (*NRT*, *NR*, *AMT*, *nirA*) have some of the highest constitutive transcript abundances of any pathway,

exhibiting some significant directionality of gene expression under variable Fe conditions, but to a minimal extent (Fig. 4B). Some studies have suggested diatoms exhibit substantial changes in expression of protein-encoding genes involved in nitrogen metabolism, particularly in the natural environment (Marchetti et al., 2012), whereas others have likewise shown a lack of substantial change in gene expression (but not protein synthesis) in diatoms grown in culture (Cohen et al., 2018). This finding supports previous studies which suggest picoeukaryotes, and other small phytoplankton, provide a "baseline" rate of primary production under limiting conditions with a minimal response to dramatic shifts in environmental conditions (Meyer et al., 2022).

More research is needed to fully elucidate the strategies by which *Bathycoccus* adapts to iron-limited environments. *ISIP3*, an iron-starvation induced protein of poorly characterized function (Behnke and La Roche, 2020), appears to play an important role in its adaptation strategy. However, it is possible that *Bathycoccus* expresses additional genomic adaptation strategies for iron limitation that are missed from our transcriptome analysis.

4.3 Oceanographic context

Our study provides important biogeochemical characteristics of an abundant, picoeukaryote in a climatologically important oceanographic context. Meyer et al. (2022) showed that small cells (<5 µm) accounted for the majority of biomass and primary production, including new production, at Station P during the EXPORTS observation period. Furthermore, *Bathycoccus* appears to constitute a substantial proportion of this small-celled community, with 18S rDNA data indicating that *Bathycoccus* is within the top 15% of the most abundant phytoplankton generally and one of the top five most abundant genera of picoeukaryotes (Jones and Rynearson, 2022).

Our estimated rates of new production by picoeukaryotes such as *Bathycoccus* under Fe- and Fe+ conditions were compared to the average small-celled new production rates of 33.3 ± 14.4 nmol N L^{-1} d^{-1} from the NP EXPORTS campaign (Fig. 3). While higher rates of NO_3^- uptake within a culture are expected relative to a mixed, in situ community and thus, may account for the discrepancy, overall, our analysis suggests that *Bathycoccus* may contribute substantially to new production at Station P, especially when iron concentrations are able to support higher growth rates and cellular nitrogen quotas.

With projected decreases in euphotic zone nutrient concentrations in many parts of the oceans as a result of climate change (Kwiatkowski et al., 2020), induced changes in water mass stratification and overall circulation, models of future projections predict an overall shift towards dominance by smaller phytoplankton (Henson et al., 2021). Abundant, small-cell phytoplankton with streamlined genomes and enhanced capabilities to adapt to changing environmental conditions, such as *Bathyccoccus*, hold distinct advantages in future climate conditions. Further studies of *Bathycoccus* grazing rates, sinking speeds, etc. are needed to fully understand its ecology moving forward and how this will impact net carbon export rates and other trophic level interactions.

Conclusion

In low iron environments, *Bathycoccus sp.* exhibits physiological strategies, including reduced growth rates, small cell size, and metabolic restructuring, to combat Fe limitation and maintain high rates of new production and substantial abundances within its community. This study furthers our understanding of this poorly characterized picoeukaryote and serves as a case study for new production rates of small-celled phytoplankton. Here, we add to the body of knowledge reaffirming the need to shift our thinking on key phytoplankton groups that have the potential to contribute to carbon export and pay additional attention to the role

picoeukaryotes play in ecosystem dynamics generally, now and in future ocean climate scenarios.

Acknowledgements

We thank the EXPORTS Chief Scientists, D. Steinberg and J. Graff, and the Captain and crew of the *R/V* Roger Revelle for their roles in the initial sample collection, R. Paerl for use of his flow cytometer, and J. Graff for NP EXPORTS flow cytometry data. We also thank R. Flynn for her helpful comments. This work was supported by NASA Grant 80NSSC17K0552 and NSF Grant OCE2219973 to AM.

Competing Interests

The authors declare no competing interests.

Data Availability Statement

All data presented here are publicly available at the National Center for Biotechnology Information (Accession number PRJNA1072555) or the Biological and Chemical Oceanography Data Management Office (project ID: 914269).

References

Behnke, J., La Roche, J. 2020. Iron uptake proteins in algae and the role of Iron Starvation-Induced Proteins (ISIPs). European Journal of Phycology 55(3), 339-360. doi.org/10.1080/09670262.2020.1744039.

Boyd PW, Berges JA, Harrison PJ. In vitro enrichment experiments at iron-rich and poor sites in the NE subarctic Pacific. *Journal of Experimental Marine Biology and Ecology*. 1998. 227: 133–151. doi.org/10.1029/98GB00745.

Brand LE, Guillard RRL, Murphy LS. A method for rapid and precise determination of acclimated phytoplankton reproduction rates. *Journal of Plankton Research*. 1981. 3(2): 193-201. doi.org/10.1093/plankt/3.2.193.

Chisholm SW, Frankel SL, Goericke R, Olson RJ, Palenik B, Waterbury JB, West-Johnsrud L, Zettler ER. *Prochlorococcus marinus* nov. gen. nov. sp.: an oxyphototrophic marine prokaryote containing divinyl chlorophyll *a* and *b*. *Arch. Microbiol*. 1991. 157:297-300.

Cohen NR, Gong W, Moran DM, McIlvin MR, Saito MA, Marchetti A. Transcriptomic and proteomic responses of the oceanic diatom Pseudo-nitzschia granii to iron limitation. *Environmental Microbiology*. 2018. 20(8), 3109-3126. doi:10.1111/1462-2920.15386.

Ellis, K. 2015. The coeffects of iron and vitamin B12 on marine diatoms. ProQuest Dissertations & Theses Global. (1758252386).

Fowler BL, Neubert MG, Hunter-Cevera KR, Olson RJ, Shalapyonok A, Solow AR, Sosik H. Dynamics and functional diversity of the smallest phytoplankton on the Northeast US Shelf. *Proceedings of the National Academy of Science*. 2020. 117(22), 12215-12221. https://doi.org/10.1073/pnas.1918439117.

Fu L, Beifang N, Zhu Z, Wu S, Weizhong L. CD-HIT: accelerated for clustering the next-generation sequencing data. *Bioinformatics*. 2012. 28(23; 3150-3152. doi:10.1093/bioinformatics/bts565.

Gorbunov MY, Falkowski PG. Fluorescence induction and relaxation (FIRe) technique and instrumentation for monitoring photosynthetic processes and primary production in aquatic ecosystems. *Photosynthesis: Fundamental aspects to global perspectives*. 2004.1029-1031.

Graff, J.R., Rynearson, T.A. 2011. Extraction method influences the recovery of phytoplankton pigments from natural assemblages. *Limnology and Oceanography* 9: 129–139. doi.org/10.4319/lom.2011.9.129.

Greene, R.M., Geider, R.J., Kolber, Z., Falkowski, P.G. 1992. Iron-induced changes in light harvesting and photochemical energy conversion processes in eukaryotic marine algae. *Plant Physiology* 100: 565–575. doi:0032-0889/92/100/0565/11/$01.00/0

Henson SA, Cael BB, Allen SR, Dutkiewicz S. Future phytoplankton diversity in a changing climate. *Nature Communications*. 2021. 12:5372. https://doi.org/10.1038/s41467-021-25699-w.

Jones E, Rynearson T. Data from the EXport Processes in the Ocean from RemoTe Sensing North Pacific Campaign. National Center for Biotechnology Information (NCBI). 2022. (Version 1) https://www.ncbi.nlm.nih.gov/bioproject/796004 [accessed 08/10/2024].

Kwiatkowski L, Torres O, Bopp L, Aumont O, Chamberlain M, Christian JR, Dunne JP, Gehlen M, Ilyina T, John JG, Lenton A, Li H, Lovenduski NS, Orr JC, Palmieri J, Santana-Falcon Y, Schwinger J, Seferian R, Stock CA, Tagliabue A, Takano, Y, Tjiputra J, Toyama K, Tsujino H, Watanabe M, Yamamoto A, Yool A, Ziehn T. Twenty-first century ocean warming, acidification, deoxygenation, and upper-ocean nutrient and primary production decline from CMIP6 model projections. *Biogeosciences*. 2020. 17(13), 3439-3470. https://doi.org/10.5194/bg-17-3439-2020.

La Roche J, Geider RJ, Graziano LM, Murray H, Lewis K. Induction of specific proteins in eukaryotic algae grown under iron-, phosphorus-, or nitrogen-deficient conditions. *Journal of Phycology*. 1993. 29, 767-777. doi:http://dx.doi.org/10.1111/j.0022-3646.1993.00767.x.

Le Gall F, Rigaut-Jalabert F, Marie D, Garczarek L, Viprey M, Gobet A, Vaulot D. Picoplankton diversity in the South-East Pacific Ocean from cultures. *Biogeosciences*. 2008. 5, 203-214. https://doi.org/10.5194/bg-5-203-2008.

Lelandais G, Scheiber I, Paz-Yepes J, Lozano J, Botebol H, Pilatova J, Zarsky V, Leger T, Blaiseau P, Bowler C, Bouget F, Camadro J, Sutak R, Lesuisse E. Ostreococcus tauri is a new model green alga for studying iron metabolism in eukaryotic phytoplankton. *BMC Genomics*. 2016. 17:319. doi:10.1186/s12864-016-2666-6.

Marchetti A, Juneau P, Whitney FA, Wong C, Harrison PJ. Phytoplankton processes during a mesoscale iron enrichment in the NE subarctic Pacific: Part II- Nutrient utilization. *Deep Sea Research II*. 2006. 53, 2114-2130. doi:http://dx.doi.org/10.1016/j.dsr2.2006.05.038.

Marchetti A, Schruth DM, Durkin CA, Parker MS, Kodner RB, Berthiaume CT, Morales R, Allen AE, Armbrust EV. Comparative metatranscriptomics identifies molecular bases for the physiological responses of phytoplankton to varying iron availability. *Proceedings of the National Academy of Sciences*. 2012. 109(6), E317-E325. doi.org/10.1073/pnas.1118408109.

Martin JH, Fitzwater S. Iron deficiency limits phytoplankton growth in the north-east Pacific subarctic. *Nature*. 1988. 331, 341-343. doi:http://dx.doi.org/10.1038/331341a0.

McNair, H., Meyer, M.G., Lerch, S., Maas, A.E., Stephens, B., Fox, J., Buck, K.N., Burns, S.M., Cetinic, I., Cohn, M., Durkin, C., Gifford, S., Gong, W., Graff, J.R., Jones, E.L., Santoro, A.E., Shea, C.H., Stamieszkin, K., Steinberg, D.K., Marchetti, A., Carlson, C.A., Menden-Deuer, S., Brzezinski, M.A., Siegel, D.A., Rynearson, T.A.

Quantitative analysis food web dynamics in a low export ecosystem. *BioRvix*. 2019. doi.org/10.1101/2023.03.17.532807.

Meyer MG, Gong W, Kafrissen SM, Torano O, Varela DE, Santoro AE, Cassar N, Gifford S, Niebergall AK, Sharpe G, Marchetti A. Phytoplankton size-class contributions to new and regenerated production during the EXPORTS Northeast Pacific Ocean field deployment. *Elementa: Science of the Anthropocene*. 2022. 10. https://doi.org/10.1525/elementa.2021.00068.

Moore LR, Post AF, Rocap G, Chisholm SW. Utilization of different nitrogen sources by the marine cyanobacteria, *Prochlorococcus* and *Synechococcus*. *Limnology and Oceanography*. 2002. 47(4):989-996.

Monier A, Worden AZ, Richards TA. Phylogenetic diversity and biogeography of the Mamiellophyceae lineage of eukaryotic phytoplankton across the oceans. *Environmental Microbiology Reports*. 2016. 8(4), 461-469. doi:10.1111/1758-2229.12390.

Moreno, C.M., Gong, W., Cohen, N.R., DeLong, K., Marchetti, A. 2020. Interactive effects of iron and light limitation on the molecular physiology of the Southern Ocean diatom Fragilariopsis kerguelensis. Limnology and Oceanography 65(7), 1511-1531. doi.org/10.101002/lno.11404.

Moreno, C.M., Lin, Y., Davies, S., Monbureau, E., Cassar, N., Marchetti, A. 2017. Examination of gene repertoires and physiological responses to iron and light limitation in Southern Ocean diatoms. *Polar Biology* 41, 679-696. doi.org/10.1007/s00300-017-2228-7.

Paerl RW, Venezia RE, Sanchez JJ, Paerl HW. Picophytoplankton dynamics in a large temperate estuary and impacts of extreme storm events. *Scientific Reports*. 2020. 10. https://doi.org/10.1038/s41598-020-79157-6.

Patro R, Duggal G, Love MI, Irizarry RA, Kingsford C. Salmon provides fast and bias-aware quantification of transcript expression. *Nature Methods*. 2017.

Peers G, Price NM. Copper-containing plastocyanin used for electron transport by an oceanic diatom. *Nature*. 2006. 441:341-344. doi:http://dx.doi.org/10.1038/nature04630.

Piganeau G, Grimsley N, Moreau H. Genome diversity in the smallest marine photosynthetic eukaryotes. *Research in Microbiology*. 2011. 162(6), 570-577. doi.org/10.1016/j.resmic.2011.04.005.

Price NM, Ahner BA, Morel FMM. The equatorial Pacific Ocean: Grazer-controlled phytoplankton populations in an iron-limited ecosystem. *Limnology and Oceanography*. 1994. 39, 520-534. http:doi.org/10.4319/lo.1994.39.3.0520.

Price, NM, Harrison, GI, Hering, JG, Hudson, RJ, Nirel, PMV, Palenik, B, Morel, FMM. Preparation and chemistry of the artificial algal culture medium Aquil. *Biological Oceanography*. 1989. 6, 443-461. doi.org/10.1080/10965581.1988.10749544.

Raven, J.A. 1988. The iron and molybdenum use efficiencies of plant growth with different energy, carbon, and nitrogen sources. *New Phytologist*, 279–287. doi.org/10.1111/j.1469-8137.1988.tb04196.x

Sharpe G, Zhao L, Meyer MG, Gong W, Burns SM, Tagliabue A, Buck KN, Santoro AE, Graff JR, Marchetti A, Gifford S. *Synechococcus* nitrogen gene loss in iron-limited ocean regions. *ISME Communications*. 2023. 3, 107. https://doi.org/10.1038/s43705-023-00314-9.

Soneson C, Love MI, Robinson MD. Differential analyses for RNA-seq: transcript-level estimates improve gene-level inferences. *F1000Research*. 2015. 4. Doi:10.12688/f1000research.7563.1.

Varela DE, Harrison PJ. Seasonal variability in nitrogenous nutrition of phytoplankton assemblages in the northeastern subarctic Pacific Ocean. *Deep Sea Research*. 1999. II 46, 2505-2538. http://dx.doi.org/10.1016/S0967-0645(99)00074-0.

Vannier T, Leconte J, Seeleuthner Y, Mondy S, Pelletier E, Aury J, de Vargas C, Sierack M, Iudicone D, Vaulot D, Wincker P, Jaillon O. Survey of the green picoalga Bathycoccus genomes in the global ocean. *Scientific Reports*. 2016. 6:37900. doi:10.1038/srep37900.

Worden AZ, Nolan JK, Palenik B. Assessing the dynamics and ecology of marine picophytoplankton: The importance of the eukaryotic component. *Limnology and Oceanography*. 2004. 49(1), 168-179. doi.org/10.4319/lo.2004.49.1.0168.

Worden AZ, Not F. Ecology and diversity of picoeukaryotes. *Microbial ecology of the Oceans*. 2008. 2, 159-205.

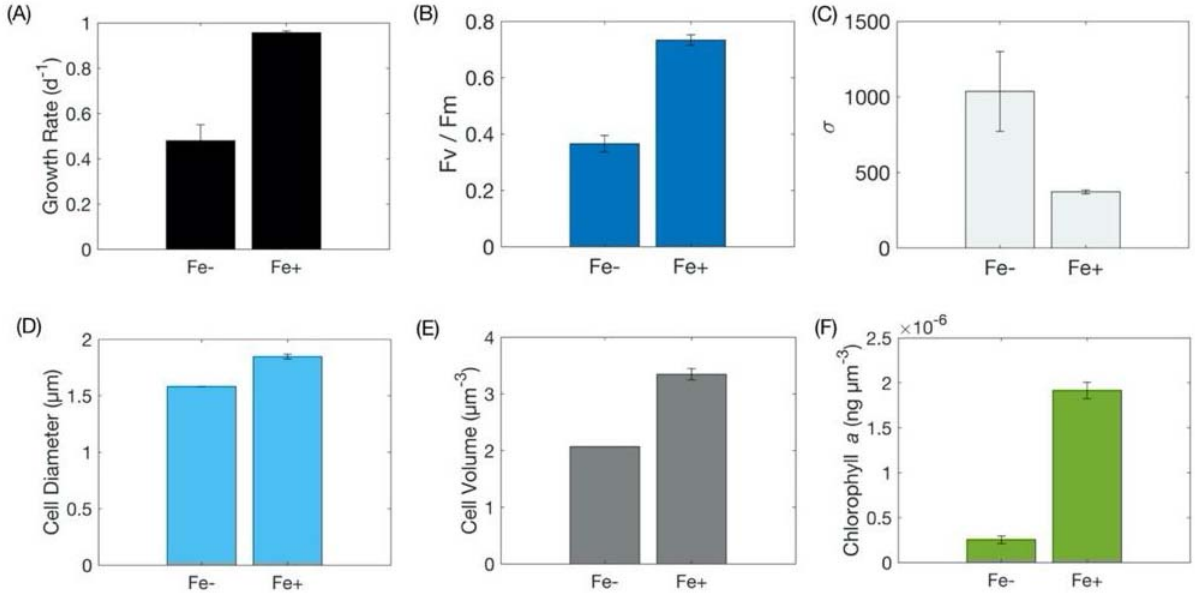

Fig. 1. Specific growth rates (A; d^{-1}), maximum photochemical efficiencies of PSII (B; Fv/Fm), PSII cross-sectional absorption areas (C; σ), cell diameters (D; µm), cell volumes (E; μm^3), and cellular chlorophyll *a* quotas (F; ng μm^{-3}) for *Bathycoccus* grown under iron-replete (Fe+) and iron-limited (Fe-) conditions. Error bars represent standard deviations with n = 3 for Fe- and n = 2 for Fe+.

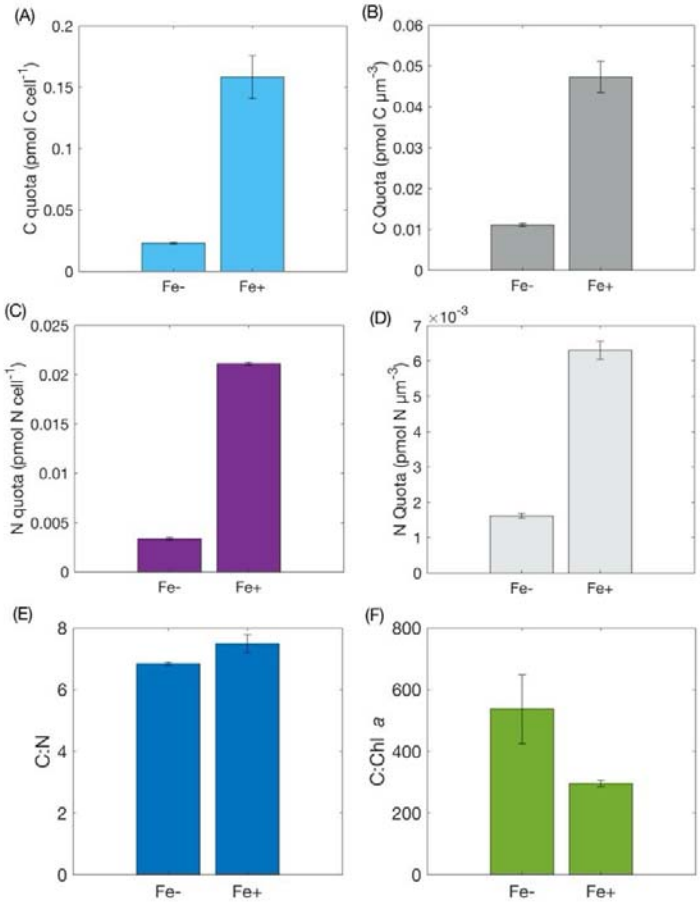

Fig. 2. Cellular carbon (A,B) and nitrogen (C,D) quotas and C:N (E) and C:Chl *a* (F) ratios for *Bathycoccus* grown under iron-replete (Fe+) and iron-limited (Fe-) conditions. Quotas are represented per cell (A,C; pmol cell^{-1}) and per cell volume (B,D; pmol µm^{-3}). Error bars represent standard deviations with n = 3 Fe- and n = 2 for Fe+.

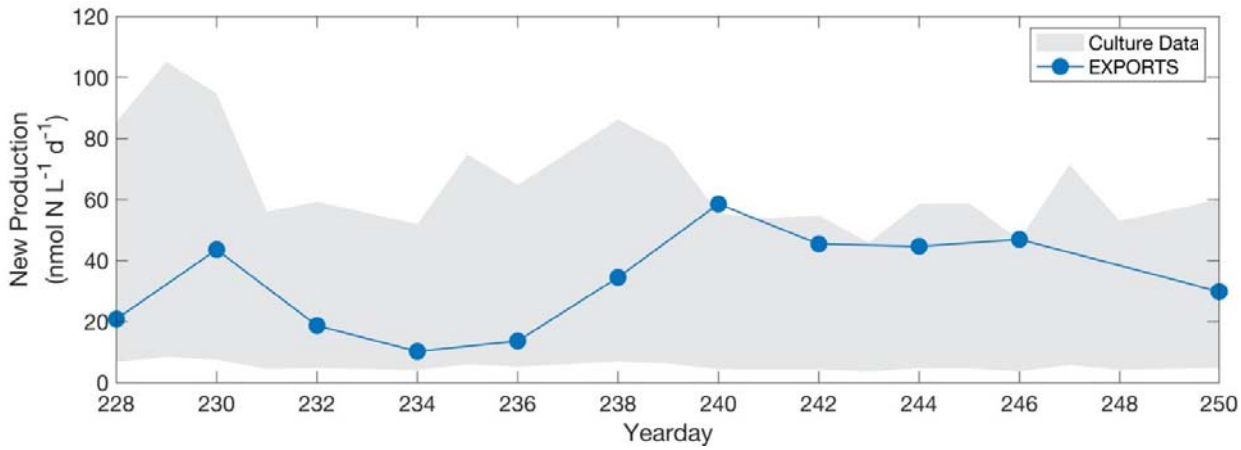
Culture Data
EXPORTS
New Production
(nmol N L^{-1} d^{-1})
Yearday
0
20
40
60
80
100
120
228
230
232
234
236
238
240
242
244
246
248
250

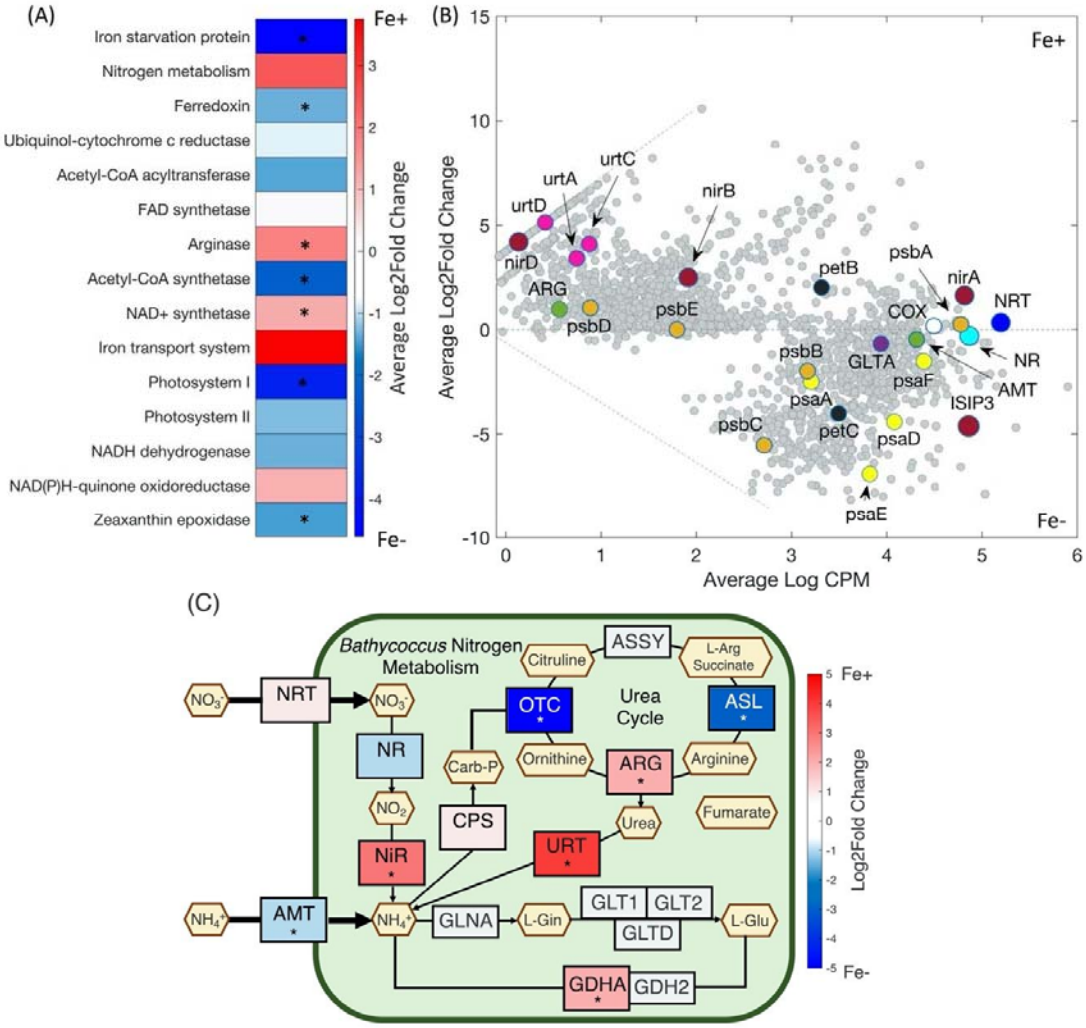

Supplemental:

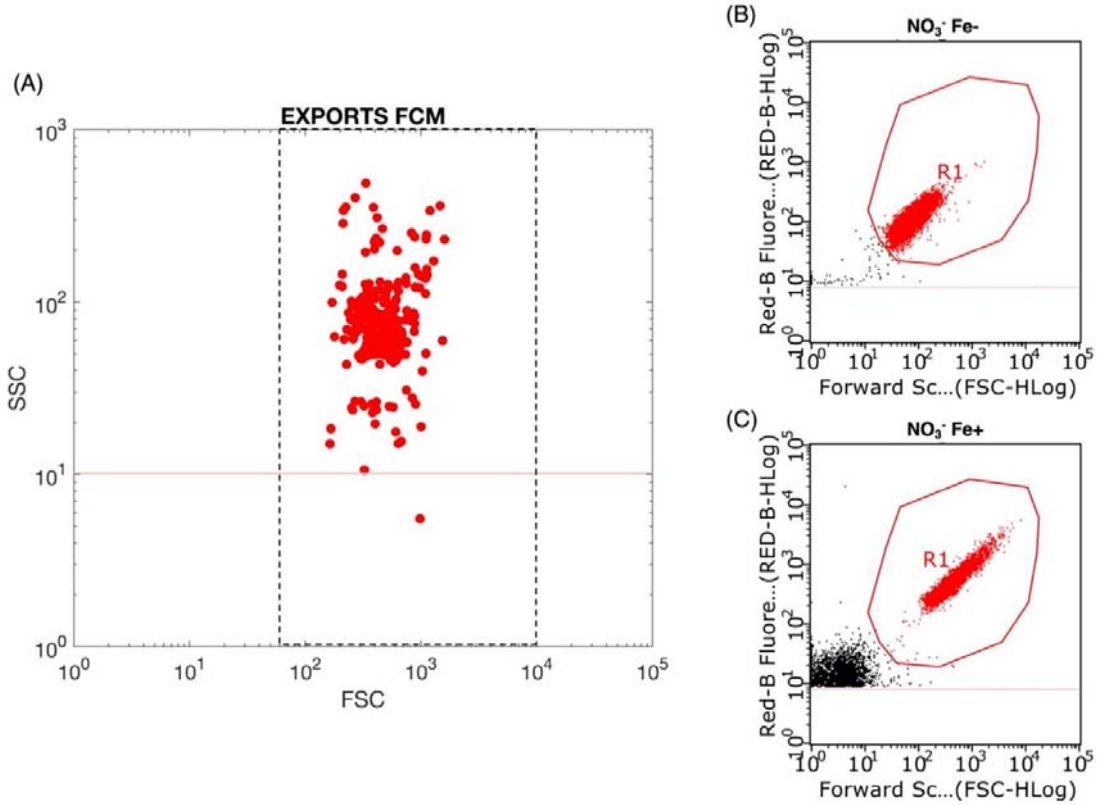

Fig. S1. Flow cytometry cytograms from (A) the North Pacific EXPORTS cruise, (B) NO_3^- Fe- samples, and (C) NO_3^- Fe+ samples. On panel A, the axes represent forward scatter (FSC) and side scatter (SSC) whereas on panels B and C, the axes represent forward scatter (FSC) and red fluorescence. The dashed box on panel A indicates the FSC gated regions (red shapes) for the culture samples.